Available online at www.sciencedirect.com
ScienceDirect
Trans. Nonferrous Met. Soc. China 25(2015) 1626−1632
Transactions of Nonferrous Metals Society of China
www.tnmsc.cn

Energy conversion of rocks in process of unloading confining pressure under different unloading paths

Guo-yan ZHAO, Bing DAI, Long-jun DONG, Chen YANG

School of Resources and Safety Engineering, Central South University, Changsha 410083, China

Received 25 May 2014; accepted 30 September 2014

Abstract: Based on energy theory and tests of rocks with initial confining pressures of 10, 20 and 30 MPa under different unloading paths, the processes of strain energy conversion were investigated. The absorbing strain energy for axial compression, the dissipating strain energy for plastic deformation and cracks propagation, the expending strain energy for circumferential deformation, and the storing and releasing elastic strain energy were considered. Unloading paths included the condition of fixing axial pressure and unloading axial pressure, increasing axial pressure and unloading confining pressure, as well as unloading axial pressure and confining pressure simultaneously. Results show that expending strain energy for circumferential deformation has mainly evolved from absorbing strain energy for axial compression in three unloading paths during unloading processes. Dissipating strain energy is significantly increased only near the peak point. The effect of initial confining pressure on strain energy is significantly higher than that of unloading path. The strain energy is linearly increased with increasing initial confining pressure. The unloading path and initial confining pressure also have great influence on the energy dissipation. The conversion rate of strain energy in three paths is increased with increasing initial confining pressure, and the effect of initial confining pressure on conversion rate of strain energy is related with the unloading paths.

Key words: unloading paths; axial pressure; confining pressure; strain energy; energy conversion

1 Introduction

Underground stope excavation results in unbalancing of rock stress. With continuous propulsion of mining face, the exposure area of surrounding rock is increasing constantly [1−3]. It causes sudden release of the elastic strain energy of rocks, which would lead to severe rock failure, such as rock burst, spalling, collapse and other geological disasters. Therefore, based on energy theory, the mechanical behavior of rock during loading has been widely investigated by means of laboratory experiment and numerical modeling, for example, energy feature under uniaxial compression, release of energy, and the relationship of deformation, confining pressure and energy [4−11].

However, investigations indicated that rock behavior under unloading is different from that under loading [12−17]. In order to better understand the mechanical properties of unloading, many experts and scholars have made great efforts on the research of this issue, and have obtained many worthy achievements, such as, deformation modulus of rock mass under different unloading rates; energy dissipation of rock in the process of unloading confining pressure [18−29]. But in the previous studies, different initial stresses and different unloadings path were not considered together to research the release and dissipation of energy in unloading.

The specimens were studied in the present study by means of conventional tri-axial unloading tests at different unloading paths and initial confining pressures. The strain energy conversion was researched, including absorbing strain energy for axial compression, dissipating strain energy for plastic deformation and cracks propagation, expending strain energy for circumferential deformation, storing and releasing elastic strain energy.

2 Experimental

2.1 Test conditions

The study was conducted at the Geo-Mechanical Test Center, Central South University, on the MTS815

Foundation item: Project (51324744) supported by the National Natural Science Foundation of China; Project (71380100006) supported by the Innovation Foundation of Doctoral Student in Hunan Province, China

Corresponding author: Bing DAI; Tel: +86-15367986516; E-mail: 522480124@qq.com

DOI: 10.1016/S1003-6326(15)63767-0

compression machine, under strict test conditions incorporated into the test program. The tester was a rigid machine that was produced by MTS Co. Ltd. (USA) specifically for versatile rock testing. This machine incorporated electro-hydraulic servo control with automatic pressure relief, as well as axis servo control and the measurement system.

The sample was a gray colored granitic rock with dimensions of *d*50 mm × 100 mm. 39 specimens had a longitudinal wave velocity of 3200−3800 m/s, a density of 2.5 g/cm^3 (when measured in natural water), and a uni-axial compressive strength of 80 MPa. And every test was conducted for 3 times.

2.2 Test program

The specimens were put into three groups for testing under different initial conditions as listed in Table 1. The axial pressure which is 80% of the tri-axial strength was applied in a strain-controlled way. The initial confining pressure was set to be three levels, 10, 20 and 30 MPa, respectively.

The detailed test procedures are as follows.

Group I: maintaining a constant axial pressure while decreasing confining pressure.

Group II: increasing axial pressure while decreasing confining pressure.

Group III: decreasing axial pressure and confining pressure simultaneously.

Table 1 Initial geostress condition of various rock samples

Sample number	Confining pressure/ MPa	Tri-axial strength/ MPa	Axial pressure/ MPa
S1, X1-1, X1-2, X1-3	10	237.5	190
S2, X2-1, X2-2, X2-3	20	306.5	245
S3, X3-1, X3-2, X3-3	30	362.5	290

3 Energy evolutions in process of unloading

3.1 Calculation method of strain energy

In the tri-axial tests of rocks, test machine does positive work to the specimen in the axial direction; confining pressure does negative work, due to the radial dilation of the specimen. So the strain energy U of rock in the whole process of tri-axial tests can be expressed as

$$U=U_1+U_3 \tag{1}$$

where U_1 is the absorbed strain energy due to axial compression by σ_1; U_3 is the consumed strain energy by negative work of σ_3.

The total strain energy U can be divided into two parts, the elastic strain energy U_e which is stored in the specimen, and the plasto-damage strain energy U_d which is responsible for plastic deformation and crack propagation in rock specimen. That is

$$U=U_e+U_d \tag{2}$$

The absorbed and consumed strain energies (U_1 and U_3) at any time during the test can be obtained by integral of the stress–strain curve as follows:

$$U_1=\int_0^{\varepsilon_1^t}\sigma_1 \mathrm{d}\varepsilon_1 \tag{3}$$

$$U_3=2\int_0^{\varepsilon_3^t}\sigma_3 \mathrm{d}\varepsilon_3 \tag{4}$$

where ε_1^t and ε_3^t are the axial and radial strain at time t, respectively.

The integral in Eqs. (3) and (4) are normally calculated in practice through area summation of tiny trapezoids, according to the definition of integral calculation. That is

$$U_1=\sum_{i=1}^{n}\frac{1}{2}(\sigma_1^i+\sigma_1^{i+1})(\varepsilon_1^{i+1}-\varepsilon_1^i) \tag{5}$$

$$U_3=\sum_{i=1}^{n}(\sigma_3^i+\sigma_3^{i+1})(\varepsilon_3^{i+1}-\varepsilon_3^i) \tag{6}$$

where n is the total number of trapezoids of stress–strain curve, and i is the segmentation points.

The elastic strain energy U_e at any time under the condition of conventional tri-axial compression can be obtained as follows:

$$U_e=\frac{1}{2E_u^t}[\sigma_{1t}^2+2\sigma_{3t}^2-2\mu_u^t(2\sigma_{1t}\sigma_{3t}+\sigma_{3t}^2)] \tag{7}$$

where E_u^t and μ_u^t are the unloading modulus of elasticity and Poisson ratio at time t, respectively.

3.2 Evolution way of strain energy in process of unloading

3.2.1 Group I

Figure 1 presents the stress–strain curves of Group I. As shown in Fig. 1, the axial strain increases from 0.0045 to 0.007, and the lateral strain increases from −0.001 to −0.011. So lateral strain increases sharply, which is 3−5 times quicker than that of the axial strain.

Energy conversion chart of Group I is shown in Fig. 2. In the process of unloading confining pressure, because the axial pressure keeps constant, the elastic strain energy U_{ei} which is the enclosed area by purple lines is equal to the elastic strain energy U_{ej} which is the enclosed area by black lines. Test machine does positive work to specimens in the axial direction. Confining pressure does negative work in lateral direction in process of unloading. So dissipating strain energy of

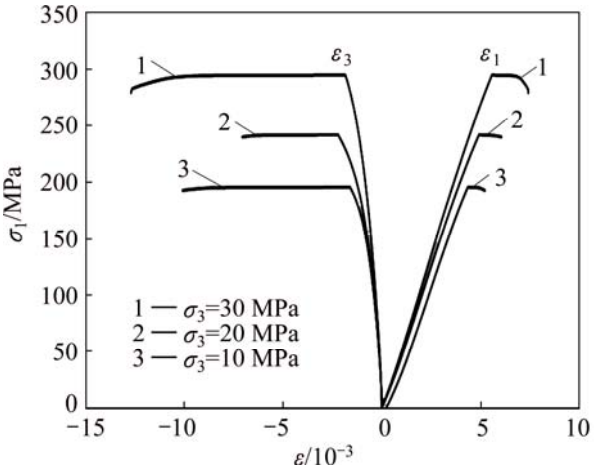

Fig. 1 Complete stress−strain curves of rock in Group I

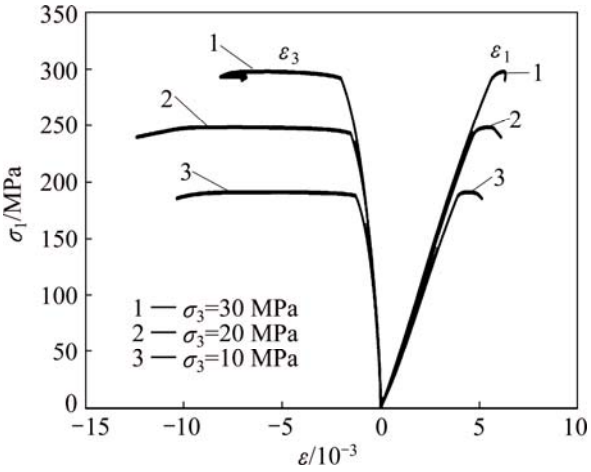

Fig. 3 Complete stress−strain curves of rock in Group II

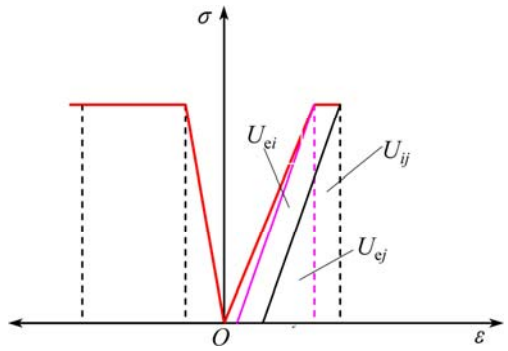

Fig. 2 Energy transformation in Group I

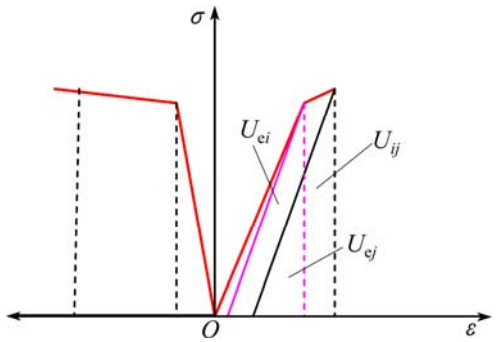

Fig. 4 Energy transformation in Group II

specimens in Group I can be obtained as follows:

$$U_{dij}=U_{ij}+2\int_{\varepsilon_{3j}}^{\varepsilon_{3i}}\sigma_3 d\varepsilon_3=\int_{\varepsilon_{1j}}^{\varepsilon_{1i}}\sigma_1 d\varepsilon_1+2\int_{\varepsilon_{3j}}^{\varepsilon_{3i}}\sigma_3 d\varepsilon_3 \quad (8)$$

where U_{ij} is the area enclosed by purple dotted lines and black dashed lines in Fig. 2.

3.2.2 Group II

Figure 3 presents the stress–strain curves of Group II. As shown in Fig. 3, the specimens show obvious lateral expansion which is more obvious than that in Group I in the process of unloading. This is mainly because more energy is provided by increasing axial compression to specimens, and the rock sample is broken without enough time to dilatate.

Energy conversion chart of Group II is shown in Fig. 4. The elastic strain energy U_{ei} which is the enclosed area by purple lines is less than the elastic strain energy U_{ej} which is the enclosed area by black lines. It illustrates that rocks absorb the elastic strain in the process of unloading. So dissipating strain energy of specimens in Group II can be obtained as follows:

$$U_{dij}=U_{ei}-U_{ej}+U_{ij}+2\int_{\varepsilon_{3j}}^{\varepsilon_{3i}}\sigma_3 d\varepsilon_3 \quad (9)$$

where U_{ij} is the area enclosed by purple dotted lines and black dashed lines in Fig. 4.

3.2.3 Group III

Figure 5 presents the stress–strain curves of Group III. The lateral strain increases rapidly and axial strain increases slowly, their variation is more than that in Group I. This is because unloading in axial is equivalent to an increase of tensile stress in the lateral direction. With the development of tensile stress, crack develops rapidly from the exterior to internal. So it shows obvious lateral expansion, which would lead to the damage of specimens eventually.

Energy conversion chart of Group III is shown in Fig. 6. As shown in Fig. 6, the elastic strain energy U_{ei} which is the enclosed area by purple lines is more than the elastic strain energy U_{ej} which is enclosed area by black lines. It illustrates that rocks release the elastic strain in the process of unloading. So dissipating strain energy of specimens in Group III can be obtained as follows:

$$U_{dij}=U_{ei}-U_{ej}+U_{ij}+2\int_{\varepsilon_{3j}}^{\varepsilon_{3i}}\sigma_3 d\varepsilon_3 \quad (10)$$

where U_{ij} is the area enclosed by purple dotted lines

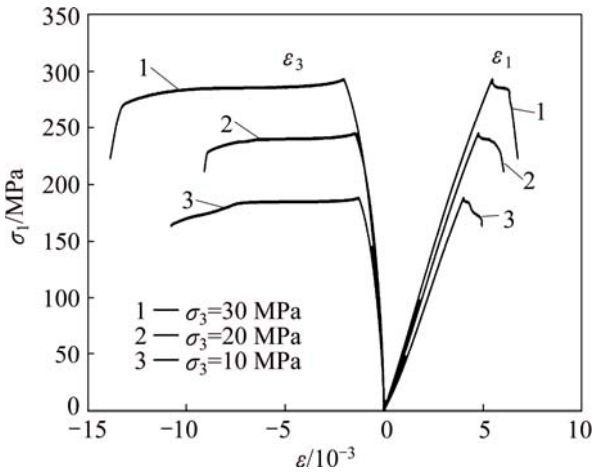

Fig. 5 Complete stress−strain curves of rock in Group III

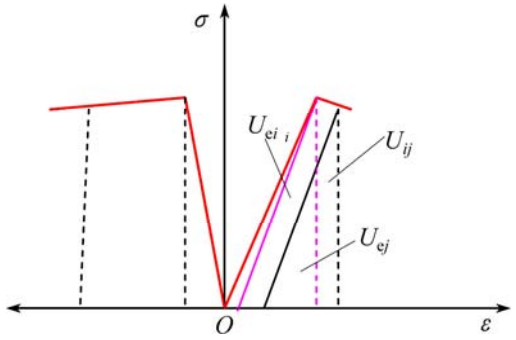

Fig. 6 Energy transformation in Group III

and black dashed lines in Fig. 6.

3.3 Analyses of evolution process of strain energy

Figure 7 presents the time history curves of strain energy accumulation, dissipation and release for specimens tested in three unloading paths. Elastic strain energy in Group I remains unchanged in the process of unloading. So the curves of elastic strain energy in Group I have not been mapped. The results can be summarized as follows.

1) In the initial stage of unloading confining pressure, absorbed strain energy U_1 for axial compression rapidly increases, while the dissipation energy U_d remains unchanged. It shows that the specimens stay in the elastic stage. The absorbed strain energy U_1' is mainly converted into the expending strain energy U_3' for circumferential deformation in Group I; In Group II, the absorbed strain energy U_1'' is mainly converted into the expending strain energy U_3'' for circumferential deformation and elastic strain energy U_e'' which is stored in specimens; In Group III, because the elastic strain energy U_e''' releases very few in the stage of unloading, the absorbed strain energy U_1''' is mainly converted into the expending strain energy U_3''' for circumferential deformation.

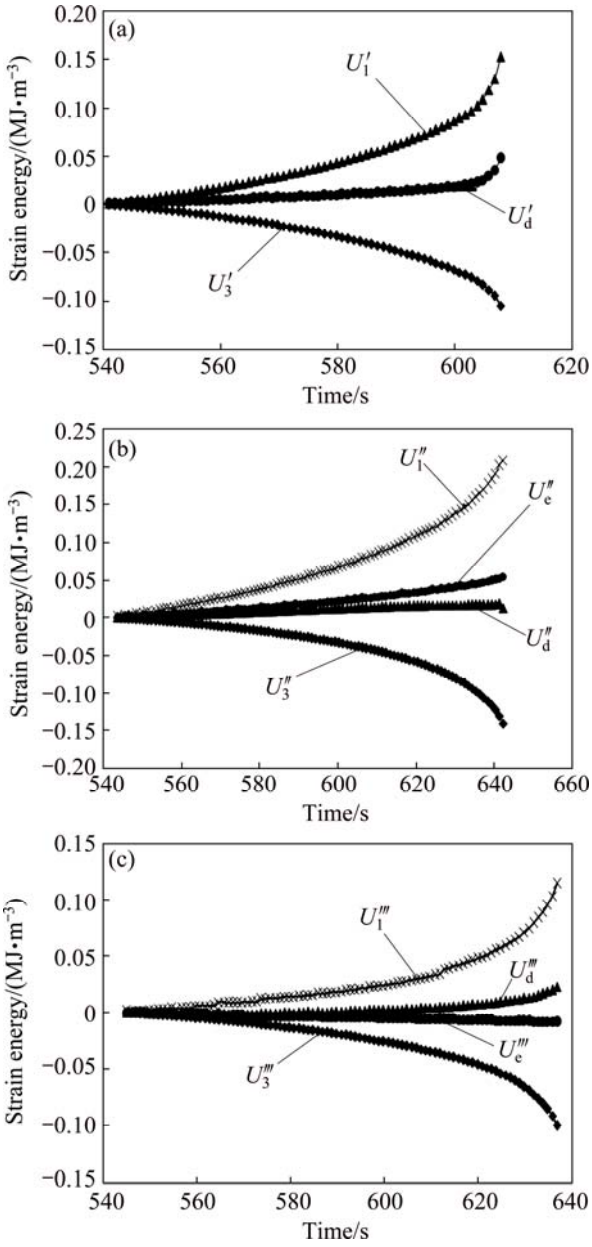

Fig. 7 Typical time-history curves of strain energy conversion for rock specimens under unloading confining pressure with initial confining pressure 20 MPa: (a) Group I; (b) Group II; (c) Group III

2) Near the peak point, the dissipation energy U_d in three groups increases quickly. This indicates that the specimen has damaged plastic deformation and crack extension. And U_e'' to be stored in the specimen in Group II reaches the highest value near the peak point. When the specimen is damaged, the elastic strain energy in specimen rapidly releases. But after the peak point, there is $U_1''+U_e''-U_3''-U_d''>0$, the residual energy may account for the rock burst, which happens sometime during unloading by excavation. And there is $0<U_1'''+U_e'''-U_3'''-U_d'''<U_1''+U_e''-U_3''-U_d''$, so the possibility of rock burst in Group III is less than that in

Group II.

Table 2 presents average strain energy at peak point during unloading. The can be summarized as follows.

1) At the peak point, U_1, U_d, U_3, U_e are all increased, positively or negatively, with the increase in confining pressure. And at the peak point, there is $U_e'' > U_e' > U_e'''$, so when the specimens are damaged, the possibility of rock burst in Group II is maximum.

2) Under the high initial confining pressure (30MPa), there is U_3''' (0.21 MJ/m^3) > U_3' (0.189 MJ/m^3) > U_3'' > (0.169 MJ/m^3), which shows that the expansion of specimens in Group III is maximum, and that in Group II is minimum.

3) The initial confining pressure has much more influence on U_1, U_3 and U_e, which is nearly linearly increased with initial confining pressure than unloading paths has. The stored elastic strain energy U_e is nearly linearly increased with initial confining pressure before peak point. This indicates that the pre-unloading stress state has much influence on accumulation of U_e. And the unloading path and initial confining pressure both have much influence on U_d.

Table 2 Average strain energy at near failure points of unloading tests

Group	Initial confining pressure/ MPa	U_1/ (MJ·m^{-3})	U_3/ (MJ·m^{-3})	U_e/ (MJ·m^{-3})	U_d/ (MJ·m^{-3})
I	10	0.100	−0.068	0.416	0.032
	20	0.150	−0.104	0.642	0.047
	30	0.247	−0.189	0.942	0.058
II	10	0.112	−0.068	0.446	0.019
	20	0.208	−0.141	0.676	0.021
	30	0.267	−0.169	0.975	0.049
III	10	0.033	−0.043	0.403	0.018
	20	0.101	−0.101	0.637	0.023
	30	0.165	−0.219	0.843	0.051

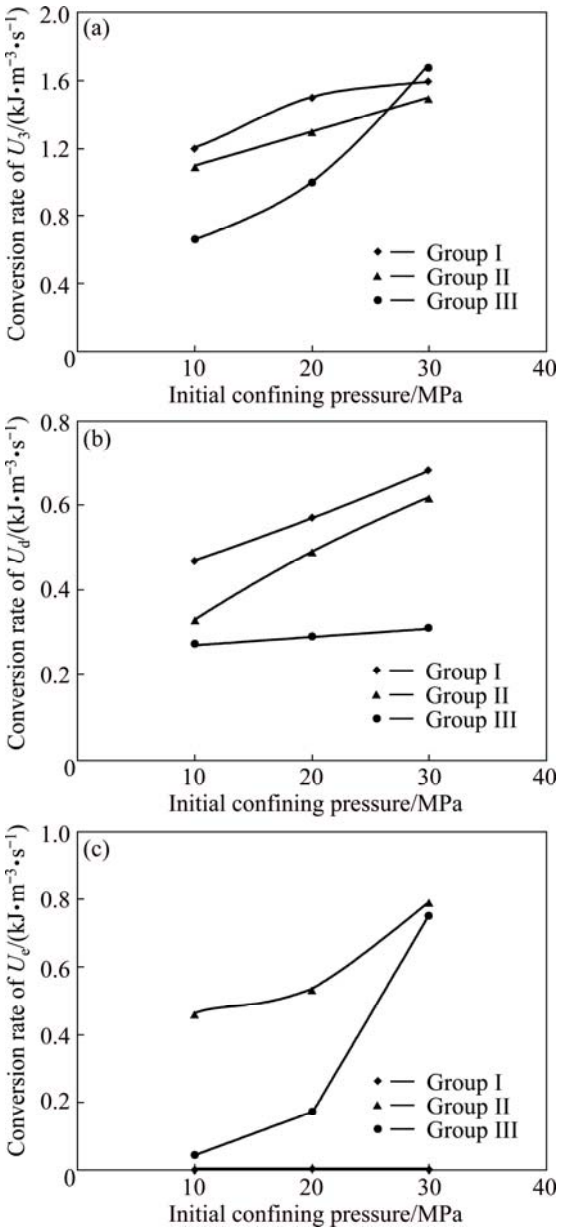

Fig. 8 Pre-peak conversion rate of strain energy for radial dilation U_3 (a), damage strain energy U_d (b) and stored elastic strain energy U_e (c)

3.4 Conversion rate

The increment of stain energy ΔU from the initial point of unloading to the peak point is divided by the elapsed time Δt to get the pre-peak conversion rate u of strain energy [24−26], that is

$$u = \frac{\Delta U}{\Delta t} \tag{11}$$

Figure 8 presents the curve of pre-peak conversion rate of strain energy versus initial confining pressure, for U_3, U_e and U_d (U_3 and U_e released take the absolute values).

1) Under low initial confining pressure (10 MPa), there is more difference about the conversion rates of expending strain energy U_3 in three groups. The conversion rate of U_3' in Group I is about two times faster than that of U_3''' in Group III. But under high initial confining pressure (30 MPa), the difference about the conversion rates of expending strain energy U_3 in three groups is not obvious. The conversion rates of U_3' and that of U_3'' are linearly increased with increasing initial confining pressure. However, the conversion rates of U_3''' is faster than that of U_3' and U_3''. This indicates that the expansion in Group III is most obvious.

2) The conversion rate of U_d is increased with initial confining pressure. And under the same confining

pressure, the conversion rate of U_d''' in Group III is minimum. Because in the process of unloading path which is decreasing axial pressure and confining pressure, the time is longer, and the absorbed strain energy U_1''' is mainly consumed by expending strain energy U_3'''.

3) The absorption rate of U_e'' in Group II and the release rate of U_3''' in Group III are increased with initial confining pressure. However, when the initial confining pressure is greater than 20 MPa, the absorption rate of U_e'' in Group II is increased obviously, indicating a sudden failure of the specimen. This is because the great amount of U_e'' has been stored in the specimen before unloading. This observation may explain severe rock burst under high geostress and quick unloading.

4) The pre-peak conversion rate of U_3 is faster than that of U_d and U_e. This may indicate that the absorbed strain energy U_1 is mainly consumed by expending strain energy U_3, while the dissipating strain energy U_d takes the least. Near the peak point, the dissipating strain energy U_d increases faster because of the plastic deformation and crack propagation.

4 Conclusions

1) Expending strain energy for circumferential deformation has mainly evolved from absorbing strain energy for axial compression in three unloading paths, and expansion in Group III is more obvious than that in Group I and Group II.

2) The influence of initial confining pressure is more significant than the unloading paths on U_1, U_3, and U_e, which is increased with the larger value of initial confining pressure.

3) In Group II, there is $U_1''+U_e''-U_3''-U_d''>0$ near the peak point, the residual energy may account for the rock burst, which happens sometimes during unloading by excavation. And there is $0<U_1'''+U_e'''-U_3'''-U_d'''<U_1''+U_e''-U_3''-U_d''$, so the possibility of rock burst in Group III is less than that in Group II.

4) The conversion rates of U_3, U_d, U_e are increased with increasing initial confining pressure. And this relationship is related with the unloading paths.

References

[1] WU Gang, SUN Jun, WU Zhong-ru. Damage mechanical analysis of unloading failure of intact rock under complex stress state [J]. Journal of Hohai University, 1997, 25(3): 44−49. (in Chinese)

[2] ZHAO Xing-dong, ZHANG Hong-xun, ZHU Wan-cheng. Fracture evolution around pre-existing cylindrical cavities in brittle rocks under uniaxial compression [J]. Transactions of Nonferrous Metals Society of China, 2014, 24(3): 806−815.

[3] LI Xi-bing, ZUO Yu-jun, WANG Wei-hua, MA Chun-de, ZHOU Zi-long. Constitutive model of rock under static-dynamic coupling loading and experimental investigation [J]. Transactions of Nonferrous Metals Society of China, 2006, 16(3): 714−722.

[4] DONG Long-jun, LI Xi-bing, ZHOU Zi-long, CHEN Guang-hui, MA Ju. Three-dimensional analytical solution of acoustic emission source location for cuboid monitoring network without pre-measured wave velocity [J]. Transactions of Nonferrous Metals Society of China, 2015, 25(1): 293−302.

[5] HE Man-cao, MIAO Jin-li, LI De-jian. Experimental study on rock burst processes of granite specimen at great depth [J]. Chinese Journal of Rock Mechanics and Engineering, 2007, 26(5): 865−876. (in Chinese)

[6] CAI Mei-feng, WANG Jin-an, WANG Shuang-hong. Analysis on energy distribution and prediction of rock burst during deep mining excavation in Ling Long gold mine [J]. Chinese Journal of Rock Mechanics and Engineering, 2001, 20(1): 38−42. (in Chinese)

[7] CAI Mei-feng, JI Dong, GUO Qi-feng. Study of rock burst prediction based on in-situ stress measurement and theory of energy accumulation caused by mining disturbance [J]. Chinese Journal of Rock Mechanics and Engineering, 2013, 32(10): 1973−1980. (in Chinese)

[8] ZUO Yu-jun, LI Xi-bing, MA Chun-de, ZHANG Yi-ping, WANG Wei-hua. Catastrophic model and testing study on failure of static loading rock system under dynamic loading [J]. Chinese Journal of Rock Mechanics and Engineering, 2005, 24(5): 741−746. (in Chinese)

[9] XIE He-ping, PENG Rui-dong, JU Yang. On energy analysis of rock failure [J]. Chinese Journal of Rock Mechanics and Engineering, 2005, 24(15): 2603−2608. (in Chinese)

[10] XIE He-ping, JU Yang, LI Li-yun. Criteria for strength and structural failure of rocks based on energy dissipation and energy release principles [J]. Chinese Journal of Rock Mechanics and Engineering, 2005, 24(17): 3003−3010. (in Chinese)

[11] LIU Guang-lian. Effect of induction unloading on weakening of rock mechanics properties [J]. Transactions of Nonferrous Metals Society of China, 2012, 22(2): 419−424.

[12] GAO Feng, ZHOU Ke-ping, LUO Xian-wei, ZHAI Jian-bo. Mechanical response of roof rock mass unloading during continuous mining process in underground mine [J]. Transactions of Nonferrous Metals Society of China, 2011, 21(12): 2727−2733.

[13] YOU Ming-qing, HUA An-zeng. Energy analysis on failure process of rock specimens [J]. Chinese Journal of Rock Mechanics and Engineering, 2002, 21(6): 778−781. (in Chinese)

[14] SU Cheng-dong, ZHANG Zhen-hua. Analysis of plastic deformation and energy property of marble under pseudo-triaxial compression [J]. Chinese Journal of Rock Mechanics and Engineering, 2008, 27(2): 273−280. (in Chinese)

[15] YANG Sheng-qi, XU Wei-ya, SU Cheng-dong. Study on the deformation failure and energy properties of marble specimen under tri-axial compression [J]. Engineering Mechanics, 2007, 24(1): 136−142.

[16] WANG Xue-bing. Unstable criterion of rock specimen subjected to shear failure in uni-axial compression based on energy principle [J]. Engineering Mechanics, 2007, 24(1): 153−156, 161.

[17] XIE He-ping, PENG Rui-dong, JU Yang. Energy dissipation of rock deformation and fracture [J]. Chinese Journal of Rock Mechanics and Engineering, 2004, 23(21): 3565−3570. (in Chinese)

[18] DONG Long-jun, LI Xi-bing, PENG Kang. Prediction of rockburst classification using random Forest [J]. Transactions of Nonferrous Metals Society of China, 2013, 23(2): 472−477.

[19] GUO Yin-tong, YANG Chun-he, FU Jian-jun. Experimental research on mechanical characteristics of salt rock under tri-axial unloading test [J]. Rock and Soil Mechanics, 2012, 33(3): 725−732. (in Chinese)

[20] CHEN Jing-tao, FENG Xia-ting. True triaxial experimental study of rock with high geostress [J]. Chinese Journal of Rock Mechanics and

Engineering, 2006, 25(8): 1537−1543. (in Chinese)
[21] GAO Yu-chun, XU Jin, HE Peng. Study of mechanical properties of marble under loading and unloading conditions [J]. Chinese Journal of Rock Mechanics and Engineering, 2005, 24(3): 456−460. (in Chinese)
[22] CHEN Wei-zhong, LU Sheng-peng, GUO Xiao-hong. Research on unloading confining pressure tests and rock burst criterion based on energy theory [J]. Chinese Journal of Rock Mechanics and Engineering, 2009, 28(8): 1530−1540. (in Chinese)
[23] HUANG Run-qiu, HUANG Da. Experimental research on mechanical properties of granites under unloading conditions [J]. Chinese Journal of Rock Mechanics and Engineering, 2008, 27(11): 2205−2213. (in Chinese)
[24] ZHU Ze-qi, SHENG Qian, XIAO Pei-wei, LIU Ji-guo. Analysis of energy dissipation in process of unloading confining pressure failure of rocks [J]. Chinese Journal of Rock Mechanics and Engineering, 2011, 30(5): 2675−2682. (in Chinese)
[25] HUANG Da, LI Yan-rong. Conversion of strain energy in tri-axial unloading tests on marble [J]. International Journal of Rock Mechanics & Mining Sciences, 2014, 66: 160−168.
[26] DONG L J, LI X B, XIE G N. Nonlinear methodologies for identifying seismic event and nuclear explosion using random forest, support vector machine, and naive bayes classification [J]. Abstract and Applied Analysis, 2014, 2014: 459137.
[27] DONG L J, LI X B. A microseismic/acoustic emission source location method using arrival times of PS waves for unknown velocity system [J]. International Journal of Distributed Sensor Networks, 2013, 2013: 307489.
[28] LI X, DONG L. An efficient closed-form solution for acoustic emission source location in three-dimensional structures [J]. AIP Advances, 2014, 4(2): 027110.
[29] DONG L, LI X, XIE G. An analytical solution of acoustic emission source location for known P wave velocity system [J]. Mathematical Problems in Engineering, 2014, 2014: 290686.

不同卸荷路径下岩石卸荷破坏的能量演化规律

赵国彦，戴 兵，董陇军，杨 晨

中南大学 资源与安全工程学院，长沙，410083

摘 要：基于岩石能量交换原理和 3 种不同卸荷路径下(恒轴压卸围压、加轴压卸围压、轴压围压同时卸载)卸围压(初始围压为 10 MPa、20 MPa、30 MPa)试验，研究卸荷条件下岩石轴向吸收应变能、环向扩容消耗应变能、弹性应变能以及耗散能的演化特征与演化速率。研究结果表明，3 个方案中，岩石轴向吸收的应变能主要转化为环向扩容消耗应变能，扩容程度为：方案 3>方案 1>方案 2，而转化为耗散能较少，只有在临近破坏时耗散能才明显增加。初始围压对轴向应变能、环向扩容消耗应变能及弹性应变能的影响程度明显大于卸载路径，且都随着初始围压的增大呈近似线性增加。卸载路径和初始围压对耗散能有显著的影响。三个方案中应变能的演化速率均随着初始围压的增大而增加，初始围压对应变能演化速率的影响与卸载路径有关。

关键词：卸荷路径；轴压；围压；应变能；能量演化

(Edited by Yun-bin HE)